MIJST
MIST International Journal of Science and Technology

Aerodynamic Characteristics and Flow Patterns of Square Cylinders with Rounded Facets

Nripendranath Biswas

Titas Gas Transmission and Distribution PLC, 105 Kazi Nazrul Islam Avenue, Kawran Bazar, Dhaka-1215, Bangladesh

Corresponding Email: *nripendranath.biswas5@gmail.com*

ARTICLE INFO

Article History:

Received: 01th May 2025
Revised: 17th June 2025
Accepted: 18th June 2025
Published: 30th June 2025

Keywords:

Cylinder with rounded facet
Angle of attack
Vortex shedding behaviour

ABSTRACT

This study experimentally investigates the effect of facet width on the static pressure distribution around a single square cylinder with rounded facets. Experiments are conducted in an open-circuit wind tunnel at a Reynolds number of 5.4×10^4, based on the side dimension of the cylinder subjected to a uniform flow velocity of 13.6 m/s. Five different dimensionless facet widths are systematically introduced to assess their influence on pressure distribution at varying angles of attack. Static pressure measurements are collected around the perimeter of the cylinder, and the resulting data are processed through numerical integration to determine the corresponding drag coefficients. The results demonstrate that incorporating facets significantly modifies the aerodynamic characteristics of the cylinder by reducing the drag coefficient compared to that of a sharp-edged configuration. The drag reduction is primarily attributed to delayed flow separation and a decrease in the size of the wake region. However, beyond a critical facet width, further increases produce only marginal improvements, indicating the presence of an optimal range for facet dimensions. This research demonstrates that facet modification is an effective and practical approach for controlling aerodynamic drag in bluff bodies. The findings offer valuable insights for optimizing structural designs subjected to wind loads, highlighting potential applications in civil engineering fields such as building design, bridge construction, and tower development. By deepening the understanding of how minor geometric alterations can impact flow behaviour, this work contributes to the development of safer, more efficient, and aerodynamically stable structures exposed to atmospheric winds.

NOMENCLATURE

C_L	Coefficient of lift
C_D	Coefficient of drag
C_P	Mean pressure coefficient
D	Width of cylinder regular to the approach flow
F_D	Drag force per unit length of the cylinder
F_L	Lift force per unit length of the cylinder
Δd	Strip width of the mid portion in the vertical direction
Δh	Strip width of the mid portion in the horizontal direction
H	Depth of cylinder in the flow direction
P	Local static pressure
P_0	Free stream static pressure
ΔP	Difference of ambient and local static pressures
ΔP_h	Pressure differences in the horizontal strip
ΔP_v	Pressure differences in the vertical strip
ρ	Density of air
U_∞	Free stream velocity
$\frac{dp}{dn}$	Pressure gradient
α	Angle of attack
γ_w	Specific weight of manometer water
R_e	Reynolds number

1. INTRODUCTION

The study of the aerodynamic properties of bluff bodies, such as square cylinders, has become a focal point in research due to their pivotal influence on the design and evaluation of civil engineering structures, including buildings and bridges. An accurate prediction of the static pressure distribution around these geometries is crucial for ensuring the structural integrity, functionality, and efficiency of such constructions. Over the years, researchers have systematically examined the pressure profiles and flow patterns around square and rectangular cylinders under various flow conditions.

Early investigations (Baines, 1963) highlighted the effects of wind velocity distribution and fluctuating loads on structural components. Subsequent studies (Lee, 1975; Mandal, 1979) detailed the pressure distributions on sharp-edged cylinders, forming a crucial basis for more advanced aerodynamic

research. Further research by scholars (Li et al., 2017) explored the influence of turbulence, illustrating how upstream flow conditions can significantly transform pressure fields around bluff bodies.

Subsequent research has focused on geometric modifications, particularly the rounding of corners, to enhance control, improve overflow separation, and optimize aerodynamic loading. Several pivotal studies (Carassale et al., 2014; Cao & Tamura, 2017) have demonstrated that corner rounding can delay flow separation, reduce drag, and alter vortex shedding behaviour. More recent investigations (Dai et al., 2017; Van Hinsberg et al., 2017; Shi et al., 2018) have employed advanced experimental techniques and numerical simulations to elucidate the complex flow structures around modified square cylinders, thereby providing deeper insights into the improvements in aerodynamic performance.

Recent parametric investigations (Vishwanath et al., 2021; Goktepeli, 2024; Solanki & Sharma, 2024; Yang et al., 2024) have systematically evaluated the effects of corner radii and chamfer ratios, demonstrating that even minor geometric modifications can substantially impact mean and fluctuating surface pressures, wake characteristics, and aerodynamic stability. Despite these comprehensive efforts, the specific influence of facet width, defined as the vertical extent of facet rounding or chamfering, on static pressure distribution has not been systematically examined. Most existing studies assume fully rounded or uniformly chamfered corners, overlooking the potential aerodynamic implications of partial or variable-width facets. In practical structural applications, facets often extend over only a portion of the cylinder width, indicating the necessity for a more detailed investigation.

This research endeavours to assess and quantify the impact of facet width on the static pressure distribution surrounding a single square cylinder with rounded facets. By methodically adjusting the facet widths while maintaining other geometric parameters constant, this study isolates and scrutinizes the effect of facet geometry on surface pressure characteristics. Utilizing established experimental techniques (Cheung et al., 1997; Li et al., 2020; Shi et al., 2018) and integrating insights from recent high-fidelity simulations (Shi et al., 2018), this research aims to provide a nuanced understanding of the relationship between localized corner modifications and their impact on aerodynamic performance. The anticipated findings are expected to enhance predictive modelling and facilitate the development of more wind-resistant design strategies for contemporary structures.

2. EXPERIMENTAL STUDY

Wind load investigation on square cylinders with rounded facets was conducted using a subsonic open-circuit wind tunnel. Five cylinders were tested, positioned downstream, and aligned with the tunnel axis at a width of 990 mm. Static pressure distribution was measured using an inclined multi-manometer. The tunnel, 5.93 m long with a 460×460 mm test section, featured a converging bell-mouth entry, a honeycomb, and two 2.25 kW axial fans. Flow velocity, controlled via a butterfly valve and measured by digital anemometer, was maintained at 13.6 m/s.

2.1 Test Section

The test was conducted at the wind tunnel's exit end in open air. A steel frame, aligned with the tunnel width, supported two plywood side walls spaced 460 mm apart, matching the tunnel's exit width. Cylinders were mounted between the side walls, with one end fastened with a bolt and the other end supported in a groove for connecting plastic tubes to the inclined manometer. Cylinders were positioned with sides parallel and front faces perpendicular to the airflow.

2.2 Constructional Details of Cylinder

For the investigation, five wooden square cylinders were constructed, each with side dimensions D = H = 60 mm, which are indicated in Figure 1. One cylinder was plain, while four cylinders had rounded facets of varying widths: 30 mm (D/2), 22.5 mm (3D/8), 15 mm (D/4), and 7.5 mm (D/8), corresponding to facet diameters of 60 mm, 62.5 mm, 75 mm, and 127.5 mm. Cylinders were mainly hollow, with a solid section for mounting, and pressure taps were made on adjacent sides, with six points per side at a 10 mm spacing. Tapings used 1.70 mm holes fitted with 1.71 mm copper tubes and connected to plastic tubes, as indicated in Figures 2 and 3. Cylinders were polished and made from seasoned teak wood to prevent deformation.

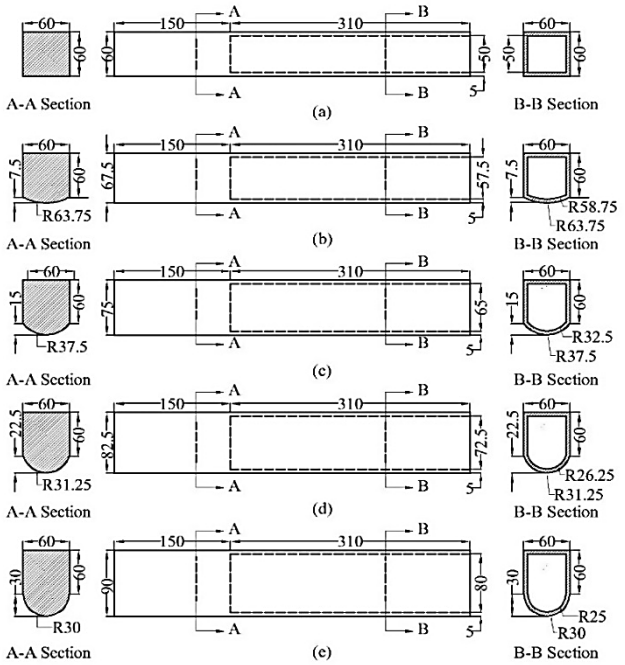

Figure 1: Sections of a square cylinder and a cylinder with a rounded facet (all dimensions are in millimetres)

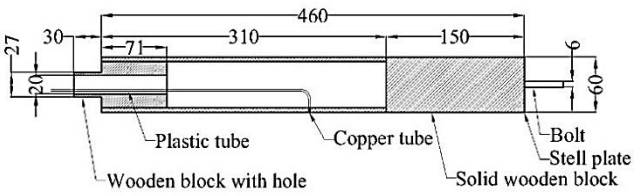

Figure 2: Sectional view of a specimen square cylinder (all dimensions are in millimetres)

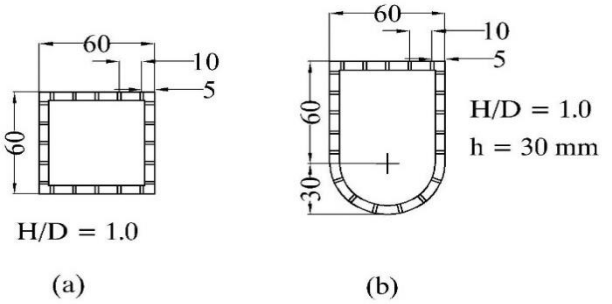

Figure 3: Tapping position on the cross-section of a square cylinder and that with a rounded facet (all dimensions are in millimetres)

2.3 Experimental Procedure

Pressure distributions were measured on a single square cylinder and a single square cylinder with rounded facets. Measurements were taken for angles of attack ranging from 0° to 45° in 5° increments for a single square cylinder and from 0° to 90° in 10° increments for a single square cylinder with rounded facets. The test was conducted at a constant flow velocity of 13.6 m/s, corresponding to a Reynolds number (Re) of 5.4×10^4, based on a diameter (D) of 60 mm. Before pressure measurements, mean velocity profiles were recorded 400 mm upstream using a pitot-static tube and an inclined manometer, confirming uniform flow across the test section, as indicated in Figure 4.

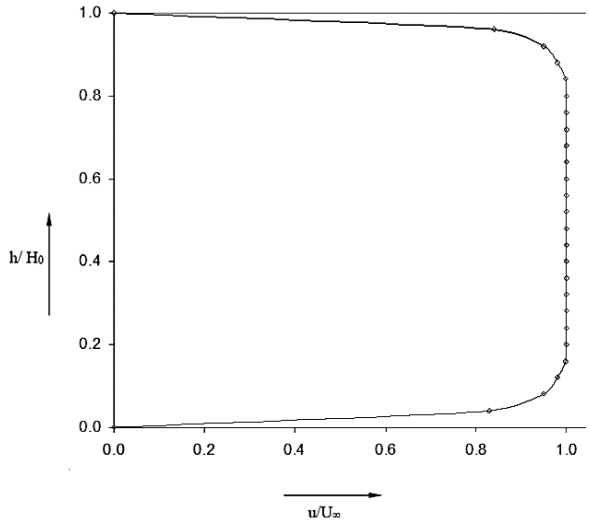

Figure 4: Velocity distribution along the width of the test section

2.4 Test of a Single Square Cylinder and Single Square Cylinder with Rounded Facets

Cylinders with D = H = 60 mm and rounded facet widths of 0 mm (flat), 7.5 mm, 15 mm, 22.5 mm, and 30 mm (facet diameters: infinity, 127.5 mm, 75 mm, 62.5 mm, 60 mm) were tested. The cylinder was centrally placed at the tunnel exit and mounted on a rotating attachment graduated from 0° to 360°, as indicated in Figure 5. The upstream flow velocity was maintained at 13.6 m/s, measured by a digital anemometer. With the cylinder's face perpendicular to the flow (0° angle of attack), static pressure distributions were recorded. Measurements were conducted from 0° to 45° in 5° increments for the cylinder without facet width, while for the other four cylinders with varying facet widths, measurements were taken from 0° to 90° in 10° increments.

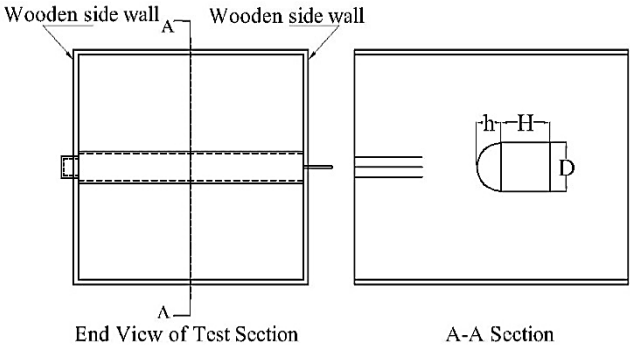

Figure 5: Tunnel test section showing the position of a single cylinder with a rounded facet

3. MATHEMATICAL MODELLING

The mathematical methodology is employed to determine the pressure coefficients and drag coefficients of a cylindrical body subjected to fluid flow. Due to constraints in the experimental setup, direct force measurement devices were not used. Instead, the coefficients were numerically determined from pressure data obtained at discrete tapping points on the cylinder surface, following a procedure similar to that of Lee, B. E. (1975). These measured values were then used to formulate expressions for the pressure and drag coefficients.

3.1 Computational procedure

To facilitate numerical analysis, the cylinder's cross-section is divided into a grid of rectangular elements. The vertical axis is segmented into six equal strips, each with a width of Δd, while the horizontal axis is divided into equal segments of width Δh. This discretization is assumed to have a negligible effect on the accuracy of the resulting pressure and drag coefficients.

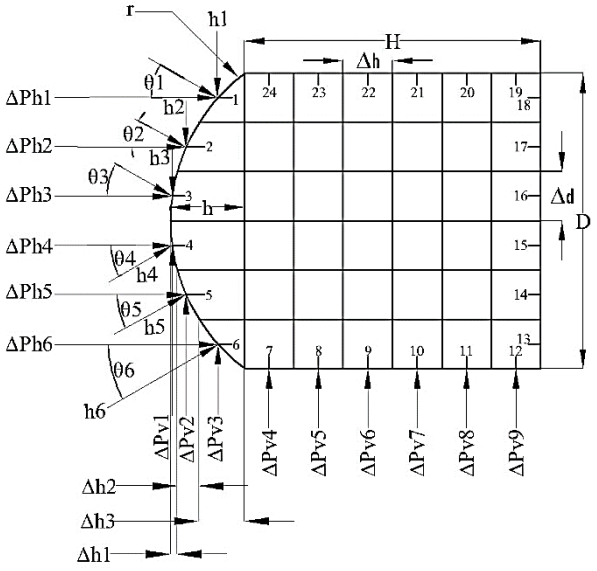

Figure 6: Section of a cylinder showing pressure tapping points and forces acting on each strip

Let ΔP_{h1} to ΔP_{h6} be respectively the pressure differences along the horizontal division between the opposite sides of

each horizontal strip, and ΔPv1 to ΔPv9 be the pressure differences in the vertical division between the opposite sides of each vertical strip. Based on the unit length of the cylinder, the area under each strip along the horizontal division is Δd × 1, while along the vertical direction is Δh × 1. However, to account for the contribution in the vertical direction from the front face, the projected areas are considered, which have non-uniform sizes, denoted by Δh1, Δh2, and Δh3, as shown in Figure 6. The horizontal and vertical components in the front face are obtained from,

$\Delta P_{h1} = h_1 \cos\theta_1 - h_{18}$ $\Delta P_{h2} = h_2 \cos\theta_2 - h_{17}$

$\Delta P_{h3} = h_3 \cos\theta_3 - h_{16}$ $\Delta P_{h4} = h_4 \cos\theta_4 - h_{15}$

$\Delta P_{h5} = h_5 \cos\theta_5 - h_{14}$ $\Delta P_{h6} = h_6 \cos\theta_6 - h_{13}$

$\Delta P_{v1} = h_4 \sin\theta_4 - h_3 \sin\theta_3$ $\Delta P_{v2} = h_5 \sin\theta_5 - h_2 \sin\theta_2$

$\Delta P_{v3} = h_6 \sin\theta_6 - h_1 \sin\theta_1$

The vertical projected width can be expressed as,

$\Delta h_1 = a\,\Delta h$, $\Delta h_2 = b\,\Delta h$ and $\Delta h_3 = c\,\Delta h$

where a, b, and c are the constants and they are dependent on the width of the front face, i.e., facet.

The other vertical components in the bottom face are obtained from,

$\Delta P_{v4} = (h_7 - h_{24})$ $\Delta P_{v5} = (h_8 - h_{23})$
$\Delta P_{v6} = (h_9 - h_{22})$ $\Delta P_{v7} = (h_{10} - h_{21})$
$\Delta P_{v8} = (h_{11} - h_{20})$ $\Delta P_{v9} = (h_{12} - h_{19})$

where, "$\theta_1, \theta_2, \ldots, \theta_6$" is the angle between the resultant and horizontal forces, and "h1, h2, …, h23, h24" are the differences between the pressure at the tapping point and the atmospheric pressure.

The drag force (F_D) is obtained by summing the horizontal and vertical components of pressure forces:

$$F_D = \gamma_w g [\Delta d \times (\Delta P_{h1} + \Delta P_{h2} + \ldots + \Delta P_{h6}) \times \cos(\alpha) + \Delta h \times (a\Delta P_{v1} + b\Delta P_{v2} + c\Delta P_{v3} + \Delta P_{v4} + \ldots + \Delta P_{v9}) \times \sin(\alpha)] \quad (1)$$

Similarly, the lift force (F_L) is computed as:

$$F_L = \gamma_w g [\Delta d \times (\Delta P_{h1} + \Delta P_{h2} + \ldots + \Delta P_{h6}) \times \sin(\alpha) + \Delta h \times (a\Delta P_{v1} + b\Delta P_{v2} + c\Delta P_{v3} + \Delta P_{v4} + \ldots + \Delta P_{v9}) \times \cos(\alpha)] \quad (2)$$

By defining: $\Delta P_h = \Delta P_{h1} + \Delta P_{h2} + \ldots + \Delta P_{h6}$, $\Delta P_v = a\Delta P_{v1} + b\Delta P_{v2} + c\Delta P_{v3} + \Delta P_{v4} + \ldots + \Delta P_{v9}$, and letting $\Delta d = \Delta h = \Delta L$, equations (1) and (2) can be simplified to:

$$F_D = \gamma_w g \Delta L (\Delta P_h \times \cos(\alpha) + \Delta P_v \times \sin(\alpha)) \quad (3)$$

$$F_L = \gamma_w g \Delta L (\Delta P_h \times \sin(\alpha) + \Delta P_v \times \cos(\alpha)) \quad (4)$$

where, $\Delta P_D = \Delta P_h \cos\alpha + \Delta P_v \sin\alpha$

Equations (3) and (4) can be written as,

$$F_D = \gamma_w \times \Delta L \times g [\Delta P_D] \quad (5)$$

$$F_L = \gamma_w \times \Delta L \times g [\Delta P_L] \quad (6)$$

where, $\Delta P_D = \Delta P_h \cos(\alpha) + \Delta P_v \sin(\alpha)$

and $\Delta P_L = \Delta P_h \sin(\alpha) + \Delta P_v \cos(\alpha)$

Turbulence intensity was not directly measured in the experiment; however, the tunnel manufacturer specifies that it is around 0.4% in the test section. A uniform velocity profile was also verified through pitot-static measurements, as presented in Figure 4.

3.2 Coefficient Calculations

Drag coefficient is defined as $C_D = \dfrac{F_D}{\frac{1}{2}\rho A U_\infty^2}$ (7)

where U_∞ is the free stream velocity.

Substituting the value of F_D from equation (5), equation (7) may be written as

$$C_D = \frac{\gamma_w \times \Delta L \times g \times \Delta P_D}{\frac{1}{2}\rho \times 6\Delta L \times U_\infty^2} \quad (8)$$

The lift coefficient is defined as $C_L = \dfrac{F_L}{\frac{1}{2}\rho A U_\infty^2}$ (9)

This can be written as, substituting the value of F_L from equation (6)

$$C_L = \frac{\gamma_w \times \Delta L \times g \times \Delta P_L}{\frac{1}{2}\rho \times 6\Delta L \times U_\infty^2} \quad (10)$$

Equations (8) and (10) are reduced to the form,

$$C_D = \frac{\gamma_w \times g \times \Delta P_D}{3 \times \rho \times U_\infty^2} \quad (11)$$

and $C_L = \dfrac{\gamma_w \times g \times \Delta P_L}{3 \times \rho \times U_\infty^2}$ (12)

Pressure coefficient is defined as, $C_P = \dfrac{P - P_0}{\frac{1}{2}\rho U_\infty^2}$, where P_0 is the ambient pressure, P is the static pressure on the surface of the cylinder, and ρ is the density of the air.

Equation (12) may be rewritten in the form,

$$C_P = \frac{\Delta P}{\frac{1}{2}\rho U_\infty^2} \quad (13)$$

The value of ΔP is obtained from $\Delta P = K \times \Delta h \times \gamma_w \times g$

where Δh is the manometer reading, K is a constant, and γ_w is the specific weight of manometric fluid.

3.3 Special Case: Zero Angle of Attack

When α = 0, the cylinder experiences a symmetric pressure distribution, resulting in a zero net lift force:

$F_L = 0$, $\Delta PL = 0$

Under this condition, the drag force and its coefficient simplify to: $F_D = \gamma_w g \Delta L \times \Delta P_h$, $C_D = \frac{2\gamma_w \times g \times \Delta P_h}{\rho \times U_\infty^2 A}$

4. RESULTS AND DISCUSSION

4.1 Pressure Distribution on the Single Square Cylinder

At zero angle of attack, the square cylinder exhibits a symmetrical flow field with a clear stagnation point located

at the centre of the front face. The pressure coefficient at this point is close to unity, indicating maximum pressure. As the angle of attack increases, this stagnation point progressively shifts toward the lower leading edge, resulting in asymmetric pressure loading and a redistribution of flow separation along the body, as presented in Figure 7.

The pressure distribution on the front surface becomes increasingly asymmetric as the angle increases. In contrast, the bottom surface, which initially experiences early separation and minimal pressure recovery at $\alpha = 0°$, begins to exhibit signs of pressure increase near the trailing edge as the angle of attack increases. At angles approaching 20 degrees, the region of highest-pressure recovery gradually shifts toward the front of the surface, indicating changes in flow reattachment and wake structure, as indicated in Figure 7.

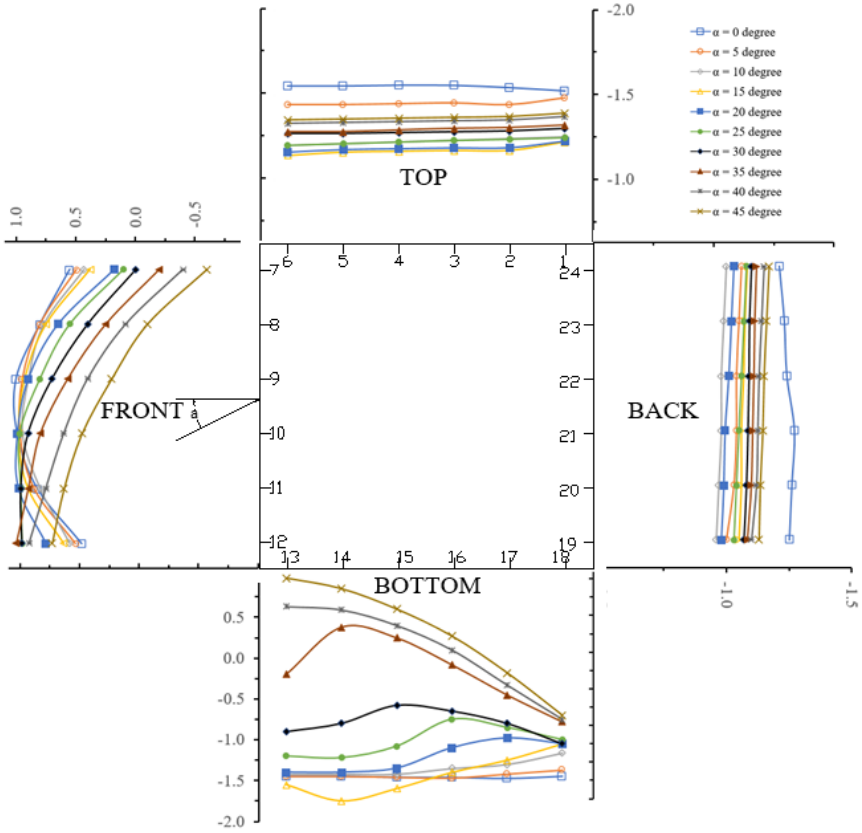

Figure 7: Pressure coefficients at various angles of attack for a cylinder with a facet width of 0.0 mm (i.e., flat)

On the top surface, the pressure remains nearly uniform across all tested angles of attack, suggesting little to no pressure recovery and consistent flow separation. On the rear surface, pressure coefficients initially increase with angle of attack up to approximately 10 degrees, indicating increased back pressure due to the displacement of vortices. Beyond this point, the pressure decreases as vortices form closer to the rear face, thereby reducing the base pressure and leading to increased drag, as shown in Figure 7.

These observations affirm that the vortex dynamics and location of the separation points are key factors influencing the surface pressure distribution. Specifically, the distance and location of vortex shedding behind the cylinder directly affect rear-face pressure and, in turn, the aerodynamic forces.

4.2 Pressure Distribution on Single Cylinder with Rounded Facets

Modifying the cylinder geometry by rounding the edges has a notable effect on the pressure distribution. For facet widths of 7.5 mm, 15.0 mm, 22.5 mm, and 30.0 mm, pressure distributions were obtained across a range of angles of attack from 0° to 90°. In contrast to the square cylinder, cylinders with rounded facets exhibit no fixed separation point. Instead, the flow separation occurs further downstream and becomes more gradual, particularly at lower angles of attack.

At zero degrees, the pressure on the front face of each rounded cylinder remains near unity at the centre, indicating effective flow stagnation. With increasing angle of attack, the stagnation points shift downward, though the transition is smoother than that observed in the square cylinder. The bottom surface initially exhibits uniform pressure, but as the angle increases, pressure recovery becomes evident toward the rear, eventually shifting forward with increasing angle, as presented in Figure 8.

On both the top and rear surfaces, the pressure coefficients display minimal variation across all tested angles, with the back pressure consistently decreasing at higher angles due to the earlier onset of flow separation and the influence of vortex shedding, as indicated in Figure 8.

It is apparent that as facet width increases, the pressure distributions begin to resemble those of the square cylinder. However, smaller facet widths promote more favourable pressure distributions, with delayed separation and enhanced pressure recovery contributing to better aerodynamic performance.

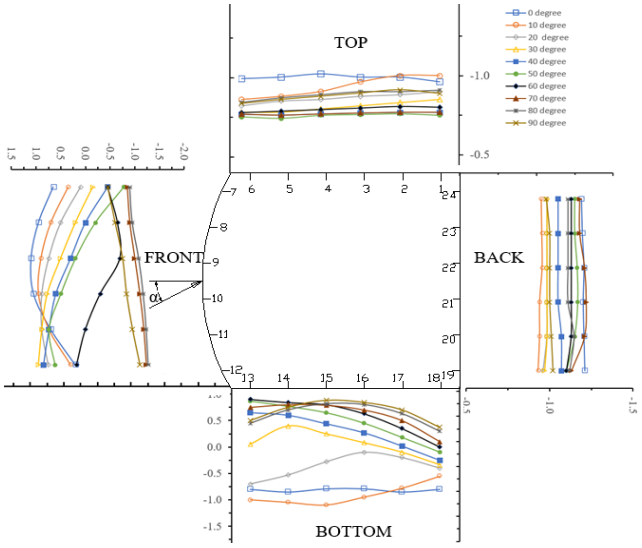

(a) Cylinder with facet width of 7.50 mm

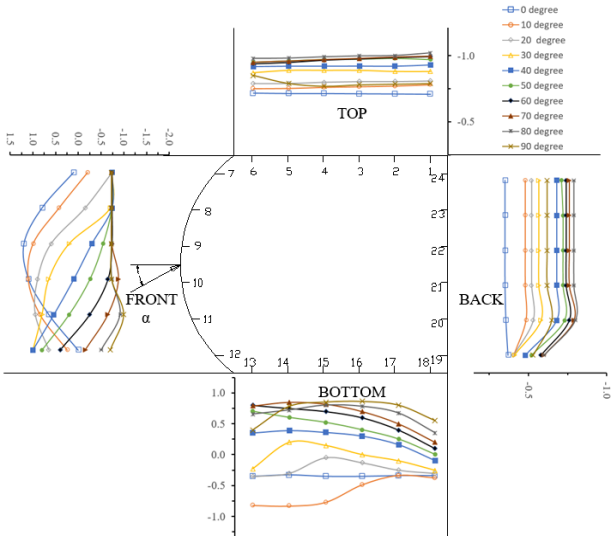

(b) Cylinder with facet width of 15.00 mm

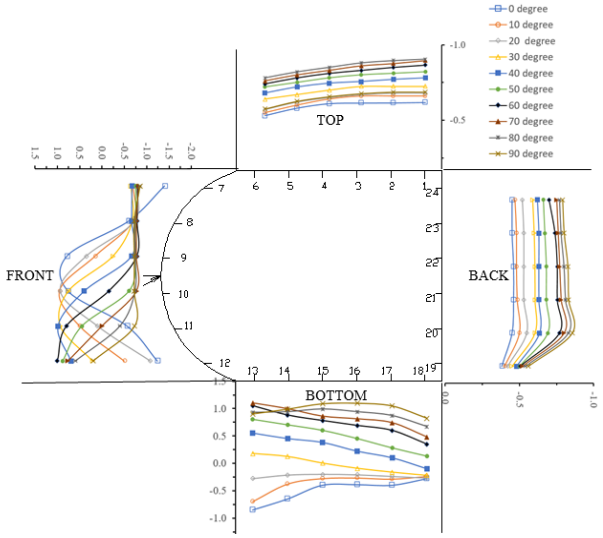

(c) Cylinder with facet width of 22.50 mm

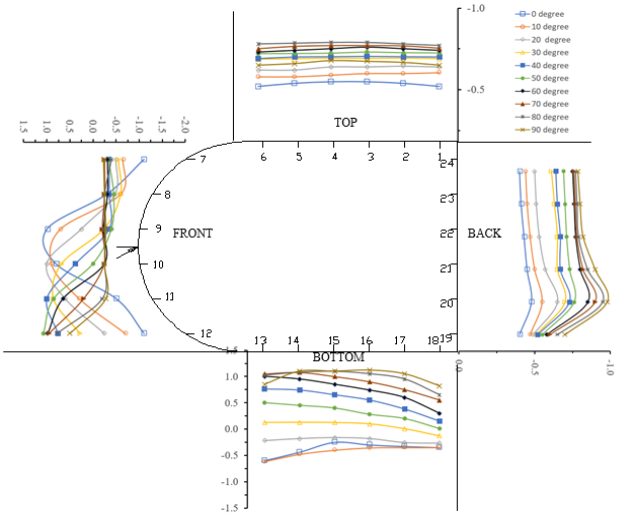

(d) Cylinder with facet width of 30.00 mm

Figure 8: Pressure coefficients at various angles of attack for a cylinder with different facet widths

4.3 Drag Coefficient Variation

The drag coefficient was determined from the integrated pressure distributions around each cylinder. For the square cylinder, drag decreases with increasing angle of attack up to approximately 12 degrees, where it reaches a minimum. This reduction is attributed to the formation of vortices further downstream, which raises the base pressure and thereby lowers the overall drag. As the angle increases beyond 12 degrees, the drag rises sharply due to the formation of vortices closer to the body, which reduces back pressure and increases resistance.

The drag coefficient trend observed for the square cylinder aligns closely with those reported by (Lee, 1975) and (Mandal, 1979), both of whom conducted similar experiments under comparable flow conditions. This agreement validates the current results and affirms the reliability of the measurement techniques, as indicated in Figure 9.

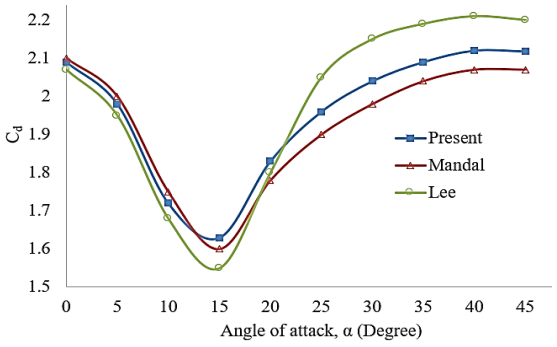

Figure 9: Variation of drag coefficient (Cd) with angle of attack (α) for a single square cylinder, showing trends consistent with those reported by (Lee, 1975) and (Mandal, 1979)

For cylinders with rounded facets, the drag behaviour varies with facet width. In the case of the 7.5 mm facet, the drag coefficient decreases up to approximately 13 degrees, then

slightly increases to around 20 degrees before declining again until about 65 degrees, after which it rises gradually up to 90 degrees. This pattern indicates that the geometry effectively delays separation and enhances pressure recovery, particularly at intermediate angles. The overall drag values remain significantly lower than those of the square cylinder across the full angle range, as presented in Figure 10.

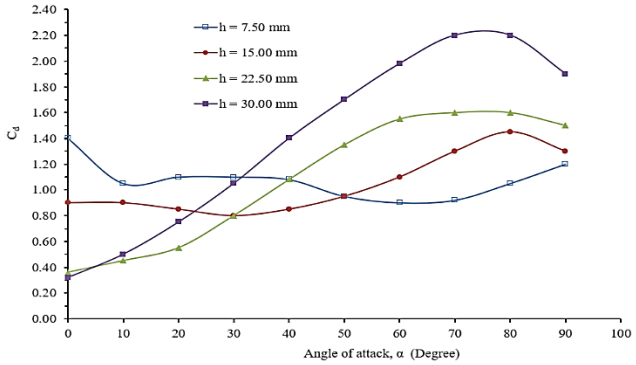

Figure 10: Variation of drag coefficient (Cd) with angle of attack (α) for a cylinder with different facet widths

For the 15.0 mm facet, a similar trend is observed, with drag decreasing up to 30 degrees and then increasing steadily. While this configuration still demonstrates lower drag than the square cylinder, the benefit is reduced compared to the 7.5 mm case. For larger facets, specifically the 22.5 mm and 30.0 mm configurations, drag increases consistently with angle of attack. The performance of these cylinders approaches that of the unmodified square cylinder, suggesting a threshold beyond which additional rounding offers limited aerodynamic gain, as shown in Figure 10.

These findings indicate that moderate facet rounding provides substantial drag reduction, while excessive rounding diminishes this benefit by reducing the influence of flow deflection and pressure gradient modification.

4.4 Lift Coefficient Variation

The lift coefficient, derived from the same pressure data, reflects the asymmetry in surface pressure and is similarly affected by changes in angle of attack and facet geometry. For the square cylinder, the lift coefficient is strongly negative at low angles of attack, resulting from the formation of a large separation bubble on the bottom surface, which generates a suction pressure differential between the upper and lower surfaces.

As the angle of attack increases, the magnitude of the lift coefficient decreases and eventually reverses direction. The results follow trends consistent with those reported (Lee, 1975) and (Mandal, 1979), with only slight discrepancies observed at higher angles due to experimental variability in separation behaviour, shown in Figure 11.

In the case of the 7.5 mm facet, the lift coefficient becomes increasingly hostile up to an angle of 45 degrees, after which it begins to recover gradually. This indicates a strong asymmetry in pressure distribution, likely due to the delayed and more controlled separation induced by the rounded edges. The 15.0 mm facet configuration exhibits a similar trend, with the maximum magnitude of negative lift occurring at approximately 50 degrees. With the 22.5 mm and 30.0 mm facets, the lift coefficient also peaks in magnitude at approximately 55° and 45°, respectively. However, the overall values are closer to those of the square cylinder, as presented in Figure 12.

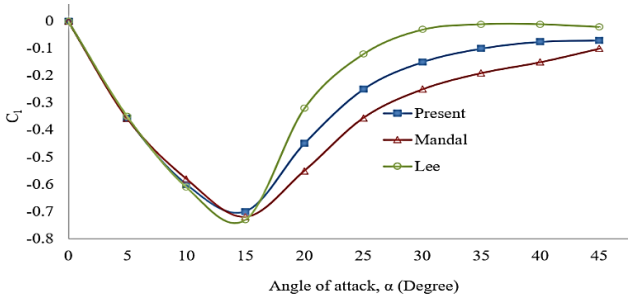

Figure 11: Variation of lift coefficient (Cl) with angle of attack (α) for a single square cylinder, showing trends consistent with those reported by (Lee, 1975) and (Mandal, 1979)

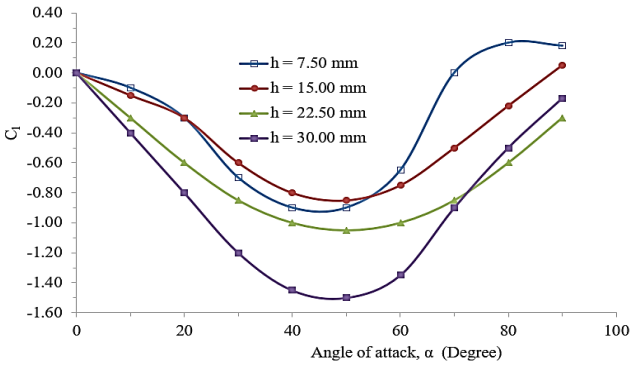

Figure 12: Variation of lift coefficient (Cl) with angle of attack (α) for a cylinder with different facet widths

These results demonstrate that moderate facet rounding enhances lift generation through increased pressure differential; however, this effect is reduced for larger facet widths, due to more uniform flow reattachment and diminished separation asymmetry.

5. CONCLUSIONS

The aerodynamic behaviour of a single square cylinder, both with and without rounded edges, was systematically analysed over a range of angles of attack. At an angle of attack (α) of 0°, the airflow remains completely separated along the top, bottom, and rear surfaces, with no reattachment detected. As the angle of attack is incrementally increased, reattachment is observed on the bottom surface, advancing from the rear corner. This shift is marked by a notable reduction in the pressure coefficient (C_P) near the front bottom corner, signifying enhanced suction.

The introduction of rounded facets plays a crucial role in reducing aerodynamic drag. As the width of the facet increases, which corresponds to a decrease in the facet radius, there is a consistent decline in the drag coefficient across all angles of attack. Notably, the configuration with a 7.50 mm facet width achieves the lowest and most stable drag values, maintaining a relatively uniform performance up to an angle of attack of α = 90°. However, once a certain facet radius is surpassed, any further reduction in drag becomes negligible.

The research findings confirm that geometric alterations, particularly facet rounding, are crucial in reducing flow separation and drag. These insights provide architects and engineers with practical design strategies to enhance the wind resistance of isolated structures, thereby improving safety and efficiency in environments prone to strong winds.

ACKNOWLEDGEMENTS

The author would like to express his gratitude to the Titas Gas Transmission and Distribution PLC, Dhaka, Bangladesh.

AUTHOR DECLARATION

The author reports no potential conflict of interest.

FUNDING

No external funding involved.

REFERENCES

Baines, W. D. (1963). Effects of Velocity Distribution on Wind Loads and Flow Patterns in Buildings. In Proceedings of the symposium on Wind Effects on Buildings and Structures,1, 197–225. Teddington, UK.

Cao, Y., & Tamura, T. (2017). Supercritical flows past a square cylinder with rounded corners. Physics of Fluids, 29(8), 085110. https://doi.org/10.1063/1.4998739

Carassale, L., Freda, A., & Marre-Brunenghi, M. (2014). Experimental investigation on the aerodynamic behavior of square cylinders with rounded corners. Journal of Fluids and Structures, 44, 195-204. https://doi.org/10.1016/j.jfluidstructs.2013.10.010

Cheung, J. C. K., Bowditch, P., Holmes, J. D., Melbourne, W. H., & Lakshmanan, N. (1997). Pressures on a scale model of the Texas Tech Building. Journal of Wind Engineering and Industrial Aerodynamics, 69–71, 529–538. https://doi.org/10.1016/s0167-6105(97)00183-9

Dai, S. S., Zhang, H. Y., & Younis, B. A. (2017). Prediction of turbulent flow around a square cylinder with rounded corners. Journal of Offshore Mechanics and Arctic Engineering, 139(3). https://doi.org/10.1115/1.4035957

Goktepeli, I. (2024). Drag reduction by the effect of rounded corners for a square cylinder. Physics of Fluids, 36(9). https://doi.org/10.1063/5.0228446

Lee, B. E. (1975). The effect of turbulence on the surface pressure field of the square prism. Journal of Fluid Mechanics, 69(2), 263–282. https://doi.org/10.1017/s0022112075001437

Li, Y., Li, C., Li, Q.-S., Song, Q., Huang, X., & Li, Y.-G. (2020). Aerodynamic performance of the CAARC standard tall building model by various corner chamfers. Journal of Wind Engineering and Industrial Aerodynamics, 202, 104197. https://doi.org/10.1016/j.jweia.2020.104197

Li, Y., Tian, X., Tee, K. F., Li, Q.-S., & Li, Y.-G. (2017). Aerodynamic treatments for the reduction of wind loads on high-rise buildings. Journal of Wind Engineering and Industrial Aerodynamics, 172, 107–115. https://doi.org/10.1016/j.jweia.2017.11.006

Mandal, A. C. (1979). A study of wind effects on square cylinders. MSc. Thesis, BUET, Dhaka.

Shi, L., Yang, G., & Yao, S. (2018). Large eddy simulation of flow past a square cylinder with rounded leading corners: A comparison of 2D and 3D approaches. Journal of Mechanical Science and Technology, 32(6), 2671–2680. https://doi.org/10.1007/s12206-018-0524-y

Solanki, D. T., & Sharma, D. S. (2024). Potential Flow Around Square Cylinder with Rounded Corners (pp. 157–172). springer nature singapore. https://doi.org/10.1007/978-981-99-6343-0_12

Van Hinsberg, N. P., Schewe, G., & Jacobs, M. (2017). Experiments on the aerodynamic behavior of square cylinders with rounded corners at Reynolds numbers up to 12 million. Journal of Fluids and Structures, 74, 214–233. https://doi.org/10.1016/j.jfluidstructs.2017.08.002

Vishwanath, N., Dwivedi, K., Saravanakumar, A., Gurugubelli, P., Murthy, K., & Sabareesh, G. (2021). A 3D numerical investigation into the effect of rounded corner radii on the wind loading of a square cylinder subjected to supercritical flow. ArXiv (Cornell University). https://doi.org/10.12989/was.2022.35.1.055

Yang, Q., Yu, C., Liu, X., Yu, W., & Jiang, H. (2024). Study on the aerodynamic characteristics and flow mechanism of square cylinders with rounded corners. Structures, 62, 106298. https://doi.org/10.1016/j.istruc.2024.106298